

Supporting Information

Activity and Selectivity in Nitroarene Hydrogenation over Au Nanoparticles on the Edge/Corner of Anatase

Liang Wang,^{*a} Jian Zhang,^a Hong Wang,^{*b} Yi Shao,^c Xiaohui Liu,^c Yan-Qin Wang,^c James P. Lewis,^b and Feng-Shou Xiao^{*a,d}

^a Key Lab of Applied Chemistry of Zhejiang Province, Department of Chemistry, Zhejiang University, Hangzhou 310028, China

^b Department of Physics and Astronomy, West Virginia University, Morgantown WV 26506-6315, USA

^c Institute of Catalysis, East China University of Science and Technology, Shanghai 200237, China

^d Key Lab of Biomass Chemical Engineering of Ministry of Education, Zhejiang University, Hangzhou 310027, China

* E-mail: liangwang@zju.edu.cn (L.W.)

* E-mail: hong.wang@mail.wvu.edu (H.W.)

* E-mail: fsxiao@zju.edu.cn (F.-S.X.)

1. Experimental Section

1.1 Reaction conditions

The reaction conditions in Figure 1A and 1B: 0.3 mmol of nitrobenzene, 10 bar of H₂, 5 mg of catalyst, 3 ml of toluene; The reaction conditions in Figure 1C: 5 mg of catalyst, H₂ pressure at 10 bar, 3 ml of toluene solvent, 80 °C; The reaction conditions in Figure 1D: 5 mg of catalyst, 0.3 mmol of nitrobenzene, 3 ml of toluene solvent, 80 °C. The reaction rates were calculated at a reaction time of 15 min.

1.2 Computational Section

In our previous study, we have established a nanoparticle-nanoparticle model to mimic the complex features of Au/TiO₂ nanosystem.¹ We utilized Au₁₃ nanocluster to represent the gold component of the complex and constructed an anatase nanostructure with both (101) and (001) surface existence, which serves as the TiO₂ substrate. On basis of our previous studies, this computational model is suitable to represent the two components and provides an insight of the interaction of the corporation between Au nanoparticles and anatase nanoparticle. After anchored on the edged/corner site, Au₁₃ interacts with the low-coordinated Ti atoms in a very strong manner, which induces oxygen vacancies forming near the attaching region, shown in Figure S1. Inspired by previous studies, we are interested to reveal the catalytic reactivity of nanostructural Au/TiO₂ in a more general way. Thus, we furthered our study by implementing the Fukui Function in the computational method.

The frontier orbital theory proposed by Fukui^{2,3} provides a general qualitative approach to understand and interpret the chemical reactions. According to the FO theory, the distribution of electron densities of the frontier orbitals is considered as the principle factor, which reveals the conceptual behavior of a molecule with regard to an approaching reagent. Parr and Yang have rationalized the features of the frontier orbital theory within the density functional theory by using a finite difference approximation, which evaluates the first derivative of electron density $\rho(r)$ at

position r , shown as $f(r) = \left[\frac{\partial \rho(r)}{\partial N} \right]_{v(r)}$.⁴⁻⁷ Based on their definition, there are three types of Fukui Functions, $f^+(r)$, and $f^0(r)$, which are corresponding to electrophilic, nucleophilic, and radical attack respectively. Herein, we implemented the Fukui functional into our package. Since we are interested in the free-radical attack, we mainly computed the $f^0(r)$ in this study. The explicit expression of $f^0(r)$ is given as, where the N corresponds to the number of electrons in the system. Thus, we can treat the Fukui Function of the radical attack by computing the difference of the electron density of LUMO and HOMO for a finite system with N total electrons. Once we obtained the values for a given system, we can plot a 3D grid representation of the Fukui Function to describe the behavior of the different sites with respect to the approaching reagents. Therefore, the Fukui Function is a density (spatially represented) and plotted as isosurfaces on the molecular/catalyst system. $f^0(r) > 0$ means susceptible to nucleophilic attack, (such as OH^-); $f^0(r) < 0$ means susceptible to electrophilic attack (such as H^+). As shown in Figure 3A, we use yellow colored isosurface to represent positive Fukui Function and blue to represent negative Fukui Function.

In this study, we accomplished our calculations by using a package named FIREBALL, which is based on the density functional theory (DFT) with a nonlocal pseudo potential scheme.^{8,9} Two types of exchange-correlation density functional are available with FIREBALL, LDA and GGA (BLYP) exchange.¹⁰ Within the LDA, the exchange-correlation is designed to exactly reproduce the energy and potential of the uniform electronic structures. Therefore, in this work, we utilized LDA, which has been used with success in a variety of system, including our previous study regarding the Au/TiO₂ complex structures.¹¹⁻¹⁴ As for the basis set, we choose the optimized numerical local atomic orbitals. They were confined to regions limited by the corresponding cutoff radii R_c . The single numerical (SN) basis set was selected for the light elements, including H, C, N, O, with the R_c values taken as $R_c^H(s) = 3.8$ a.u., $R_c^C(s) = 4.0$ a.u., $R_c^C(p) = 4.4$ a.u., $R_c^N(s) = 3.7$ a.u., $R_c^N(p) = 4.1$ a.u., $R_c^O(s) = 3.4$ a.u., $R_c^O(p) = 3.8$ a.u. While for the metal elements (Ti and Au), we use the polarized basis

set sp^3d^5 by adding a p orbital to the minimal basis set sd^5 . The cutoff radii was $R_c^{Ti}(s) = 5.8$ a.u., $R_c^{Ti}(p) = 6.2$ a.u., $R_c^{Ti}(d) = 5.4$ a.u.; $R_c^{Au}(s) = 5.1$ a.u., $R_c^{Au}(p) = 5.5$ a.u., $R_c^{Au}(d) = 4.6$ a.u.

2. Figures & Schemes & Tables

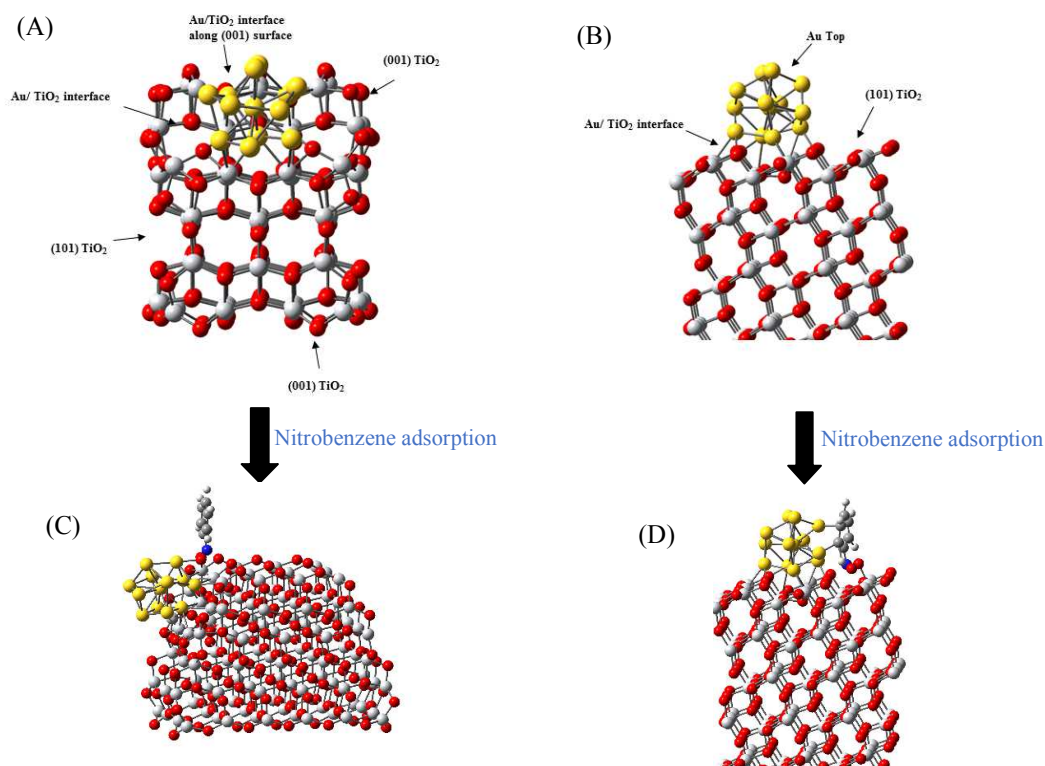


Figure S1. (A) Au₁₃/TiO₂ nanostructure with Au₁₃ cluster attached on the edge/corner sites of anatase; (B) Au₁₃/TiO₂ nanostructure with Au₁₃ cluster attached on the (101) facet of anatase; (C) Nitrobenzene molecule adsorbed on the structure A; (D) Nitrobenzene molecule adsorbed on the structure B.

The structures C and D are the two relatively lowest energetic confirmations for each trial, which includes attaching nitrobenzene on different locations on structure A and B, respectively. The adsorption energy is defined as the averaged relative adsorption energy: $E_{ads} = E_{complex} - E_{Au/TiO_2} - E_{nitrobenzene}$. By this equation, the adsorption energies (E_{ads}) of nitrobenzene on structure A and B are calculated to be -0.298 and -0.294 eV, respectively. Although the difference is not huge in quantity, it verifies the influence of Au position on TiO₂ support for adsorption of nitrobenzene molecule.

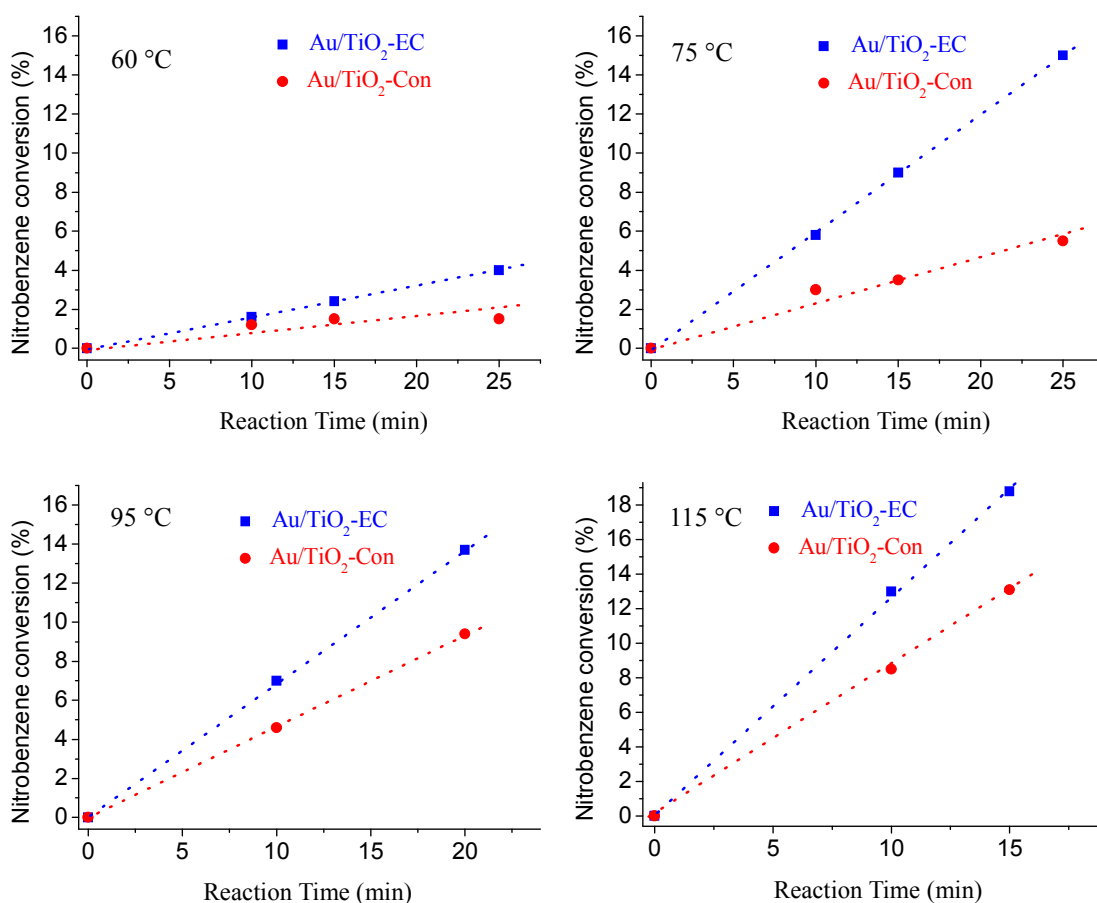


Figure S2. Dependences of nitrobenzene conversion on time over the Au/TiO₂-EC and Au/TiO₂-Con catalysts at different reaction temperatures of 60, 75, 95, and 115°C. Reaction conditions: 0.3 mmol of nitrobenzene, 10 bar of H₂, 5 mg of catalyst, and 3 ml of toluene. The straight lines are made with the best fitting of the experimental points.

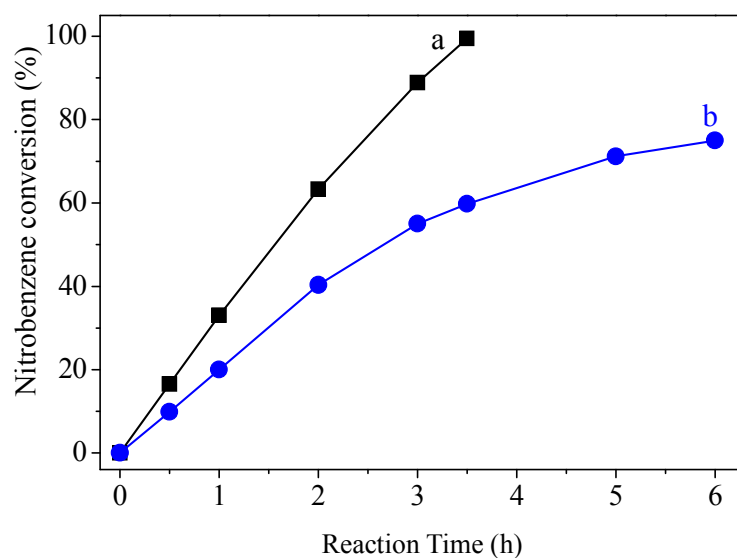


Figure S3. The dependence of nitrobenzene conversion on time over the (a) Au/TiO₂-EC and (b) Au/TiO₂-Con catalysts. Reaction conditions: 80 °C, 10 bar of H₂, 0.8 mmol of nitrobenzene, 40 mg of catalyst, and 3 ml of toluene. The selectivity to aniline is higher than 99.0%.

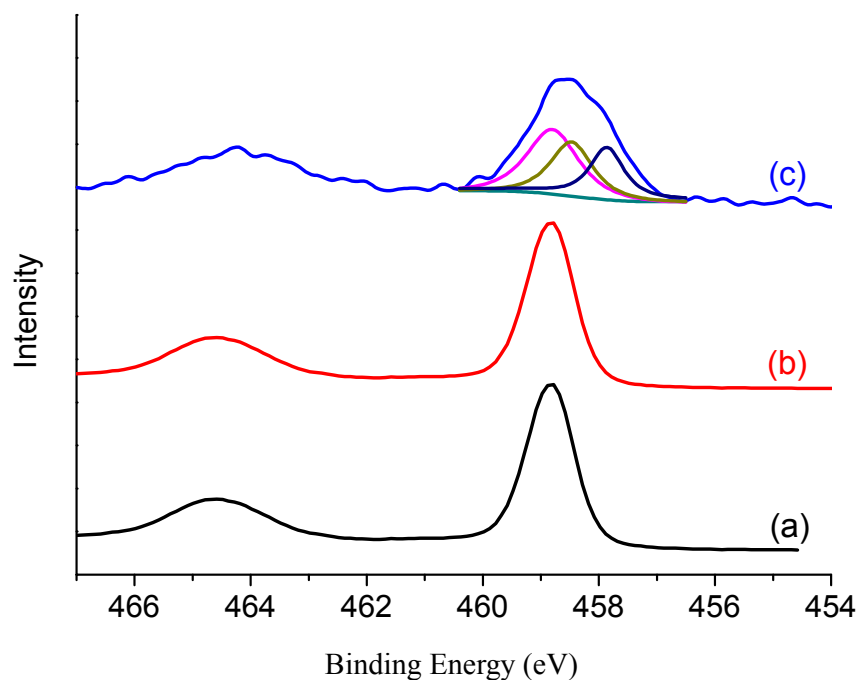


Figure S4. Au4f XPS spectra of (a) anatase, (b) Au/TiO₂-Con, and (c) Au/TiO₂-EC. The Ti2p XPS spectra of anatase and Au/TiO₂-Con exhibit Ti2p_{3/2} peak at 458.8 eV assigned to typical Ti⁴⁺ species. The Ti2p_{3/2} spectrum of the Au/TiO₂-EC shows additional peaks at 458.4 and 457.9 eV, which are attributed to the presence of electron-rich Ti species, owing to the interaction between Au and TiO₂ support.¹

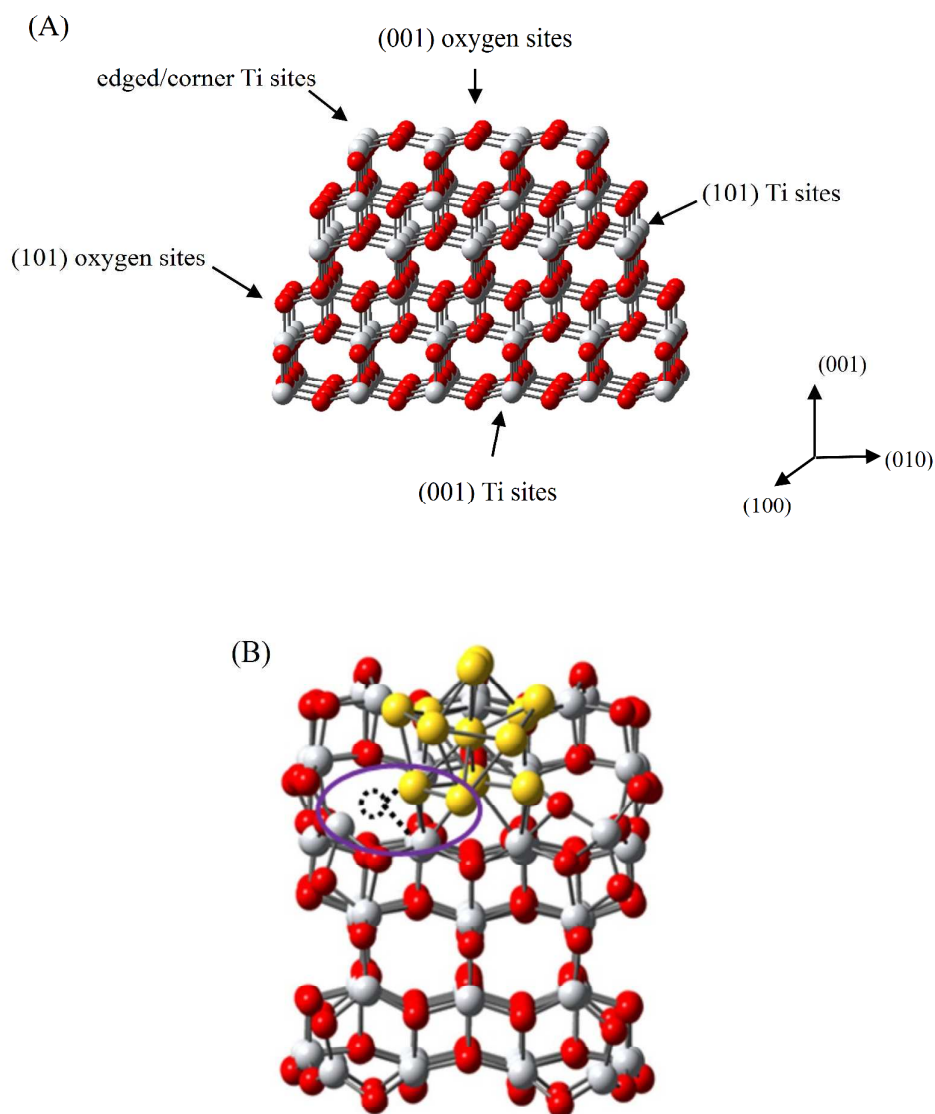


Figure S5. Computational models of (A) anatase nanostructure and (B) $\text{Au}_{13}/\text{TiO}_2$ with oxygen vacancy (Relation to $\text{Au}/\text{TiO}_2\text{-EC}$).

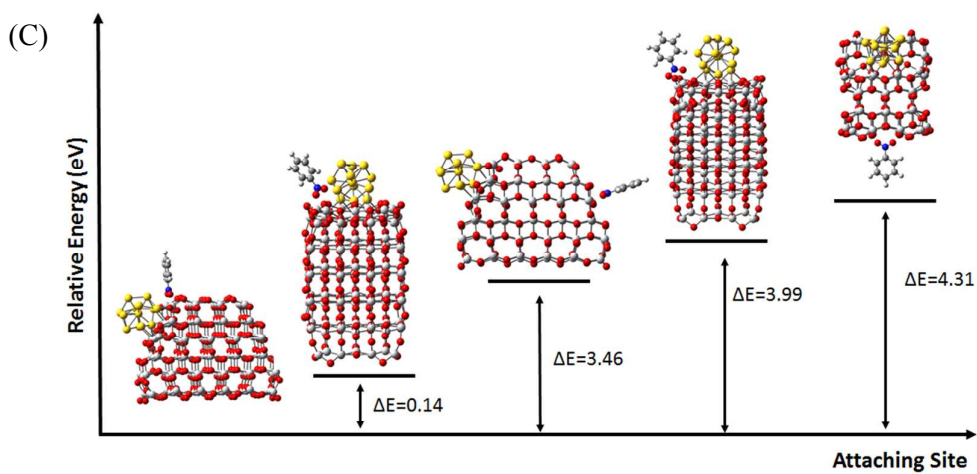
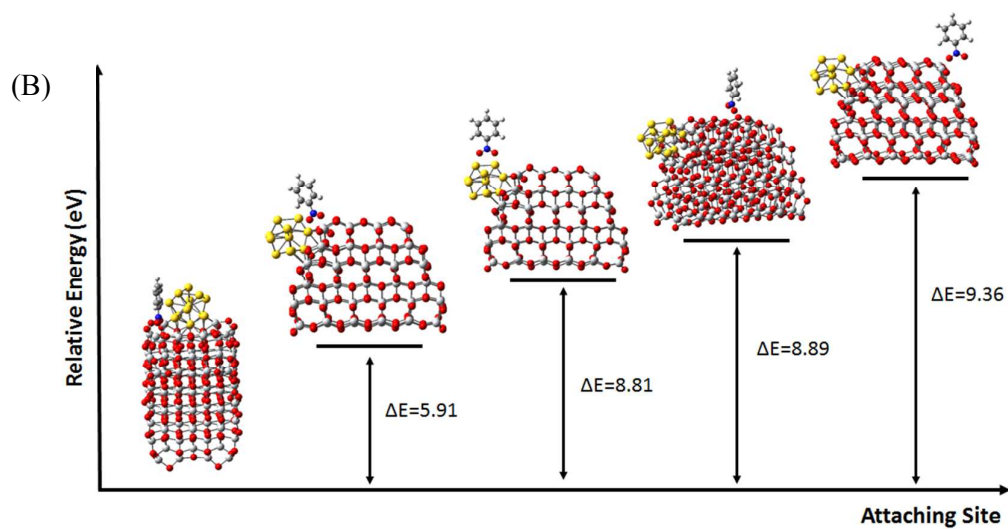
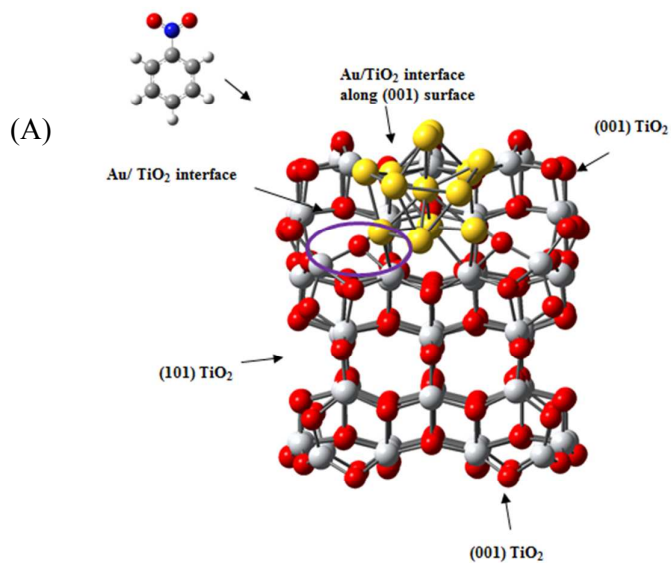


Figure S6. (A) Illustration of $\text{Au}_{13}/\text{TiO}_2$ nanostructure with Au_{13} cluster attached on the edge/corner site of anatase support, where the oxygen vacancy is labeled out by purple line; (B) The optimized structures (five lowest energetic structures) of nitrobenzene attached at different sites on the proposed $\text{Au}_{13}/\text{TiO}_2$ nanostructure; (C) The optimized structures (five lowest energetic structures) of nitrobenzene attached at different sites on the $\text{Au}_{13}/\text{TiO}_2$ nanostructure without oxygen vacancy (The $\text{Au}_{13}/\text{TiO}_2$ nanostructure in Figure S6C is the similar to that proposed in B, except the oxygen vacancy is artificially eliminated).

Herein, it is calculated several typical sites of nitrobenzene attached on $\text{Au}_{13}/\text{TiO}_2$ nanostructure, mainly including 15 adsorption sites. Five of the lowest energetic structures are presented in Figure S6B, where the difference of the relative energy between the lowest and the second lowest structure (ΔE) is 5.91 eV. Interestingly, when the oxygen vacancy of the nanostructures in Figure S6B are artificially eliminated (Figure S6C), the ΔE is only 0.14 eV, which is much lower than that on the nanostructures with oxygen vacancy (5.91 eV, Figure S6B). These results indicate the important role of oxygen vacancy in the adsorption of nitrobenzene on the $\text{Au}/\text{TiO}_2\text{-EC}$.

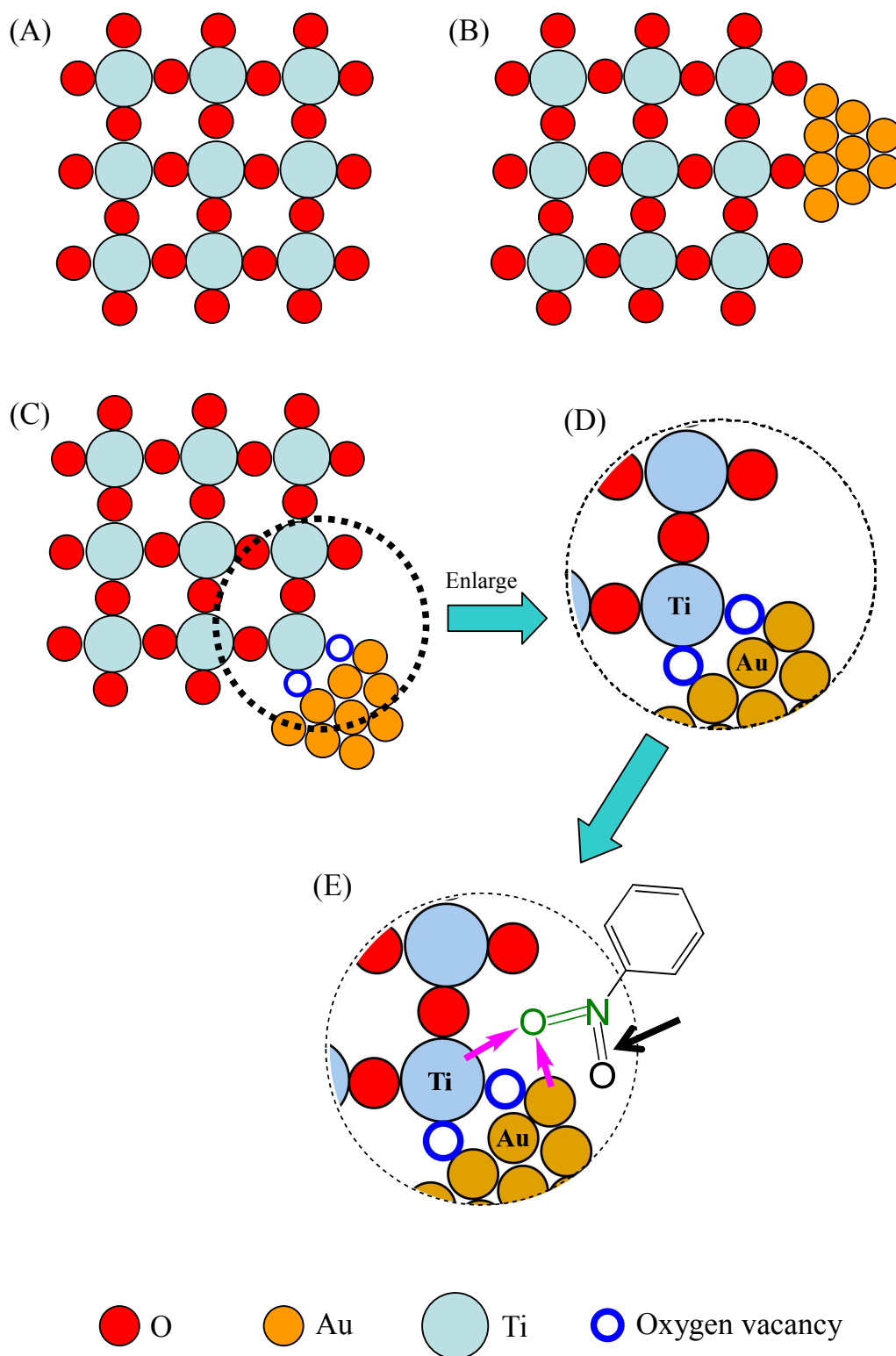


Figure S7. Sectioned view of various proposed models of (A) anatase, (B) anatase supported Au without oxygen vacancy (Relation to Au/TiO₂-Con), (C) anatase supported Au with oxygen vacancies (Relation to Au/TiO₂-EC), (D) enlarged view of

the oxygen vacancies between Ti and Au, and (E) nitrobenzene molecule adsorbed on Model (D).

As shown in Figure S7E, we found the two oxygen atoms of -NO₂ group exhibit interesting changes after attachment on the catalyst. One of the two oxygen atoms exists between one Ti atom and one Au atom (marked with dash line). The other oxygen atom only bonds to the N atom *via* a lengthened N-O bond (1.46 Å). The first oxygen atom interacts with the Ti-Au system due to the oxygen vacancy nearby, which leaves the other oxygen atom easily attacked by the hydrogen species (labeled by the black arrow in the models).

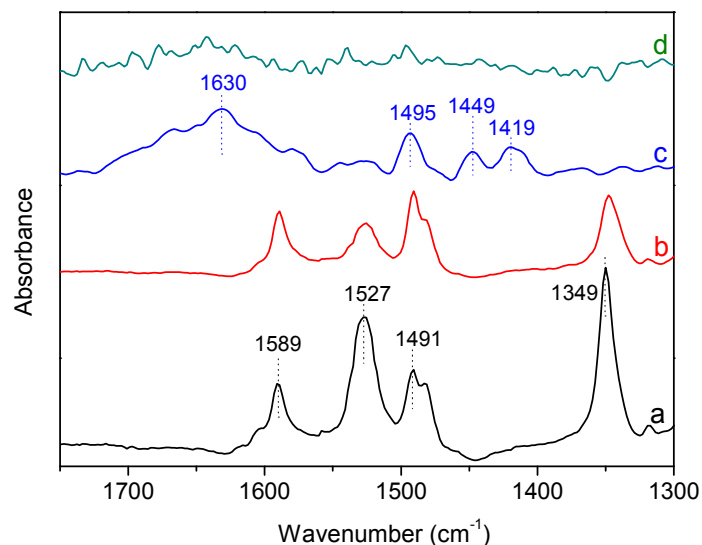


Figure S8. FT-IR spectra of (a) nitrobenzene, (b) a mixture of nitrobenzene and styrene (molar ratio at 1:1), (c) styrene adsorbed on Au/TiO₂-EC. (d) after desorption treatment of (c) at 100 °C for 10 min.

When nitrobenzene was adsorbed on the Au/TiO₂-EC, the sample exhibits bands at 1491, 1349, and 1527 cm⁻¹ related to the nitro groups (Figure S8-a). When styrene was adsorbed on the Au/TiO₂-EC, the sample exhibits bands at 1630 and 1419 cm⁻¹ associated with vinyl group, and bands at 1449 and 1495 cm⁻¹ assigned to the stretching vibrations of phenyl ring in styrene molecule (Figure S8-c). After desorption treatment at 100 °C for 10 min, the bands of styrene molecule on the Au/TiO₂-EC are nearly undetectable (Figure S8-d), which is quite different from those on the Au/TiO₂-EC (Figure 2B). These results indicate that the Au/TiO₂-EC could adsorb both of nitrobenzene and styrene molecules, but the adsorption of nitrobenzene is much stronger than that of styrene.

Furthermore, in the competitive adsorption of a mixture of styrene and nitrobenzene (molar ratio at 1:1) on the Au/TiO₂-EC, only the bands related to nitrobenzene are presented in the IR spectrum, and the bands associated with vinyl group are completely absent (Figure S8-b), indicating the high selectivity of Au/TiO₂-EC for the adsorption of nitro group than vinyl group.

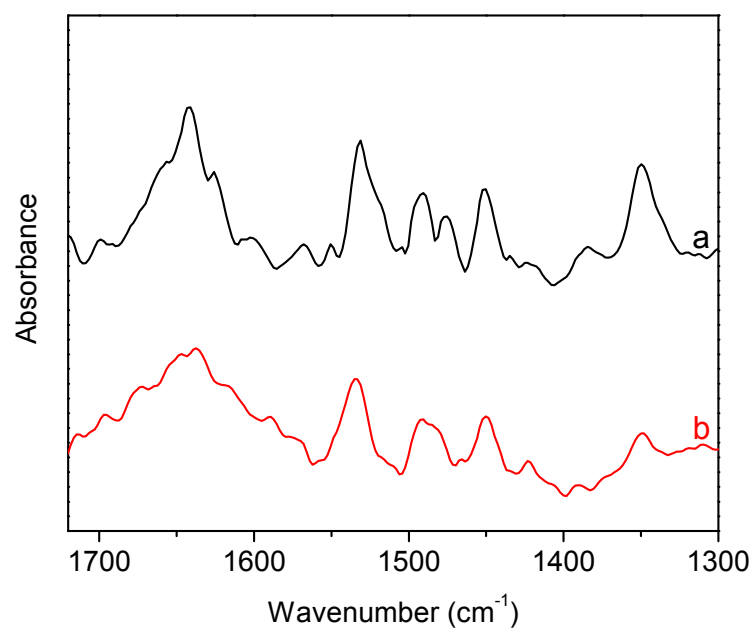


Figure S9. FT-IR spectra of (a) 3-nitrostyrene adsorbed on Au/TiO₂-EC and (b) after desorption treatment of (a) at 100 °C for 10 min.

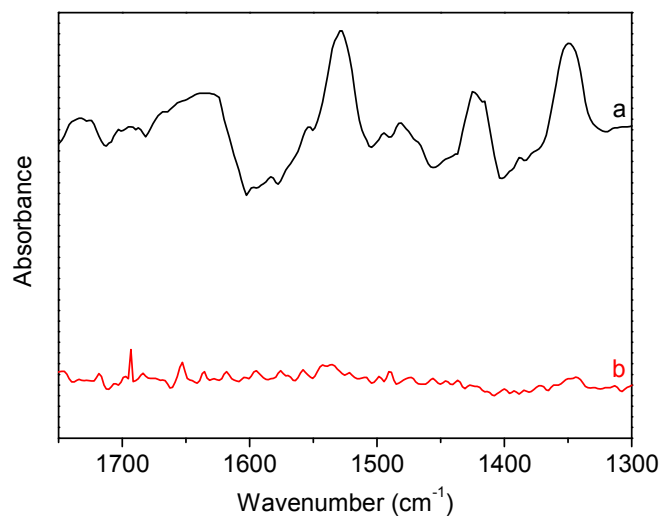


Figure S10. FT-IR spectra of (a) 3-nitrostyrene adsorbed on Au/TiO₂-Con and (b) after desorption treatment of (a) at 100 °C for 10 min.

Moreover, we carried out the adsorption of 3-nitrostyrene with both nitro and vinyl groups on the Au/TiO₂-EC. As shown in Figure S9a, the IR spectrum of Au/TiO₂-EC exhibit typical bands related to both nitro and vinyl groups. After desorption treatment at 100 °C for 10 min, the bands associated with nitro and vinyl groups still exist (Figure S9b). In contrast, most of the 3-nitrostyrene on the Au/TiO₂-Con is removed under the same desorption treatment (Figure S10). These results indicate stronger adsorption of 3-nitrostyrene on the Au/TiO₂-EC than the Au/TiO₂-Con.

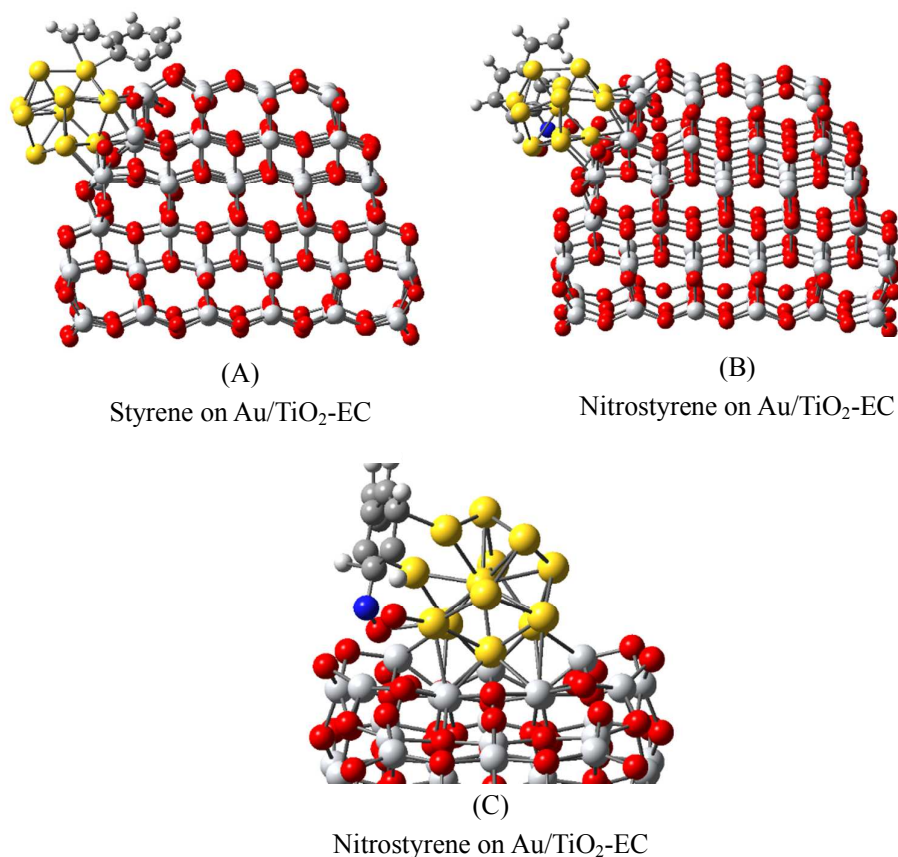
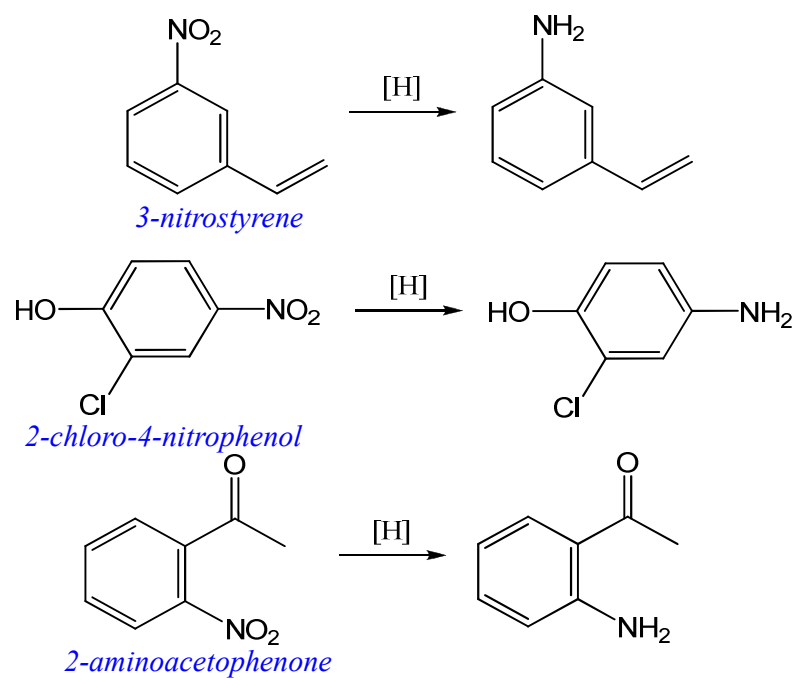
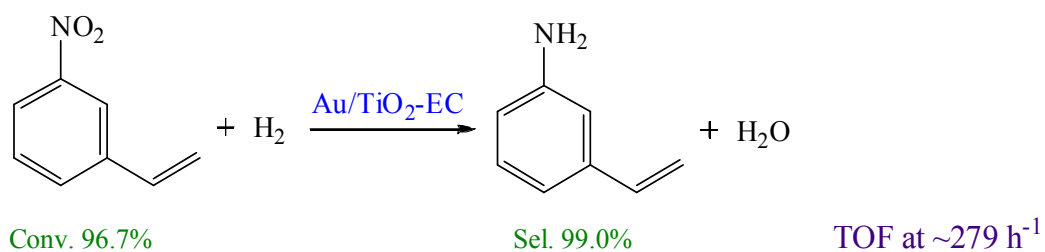


Figure S11. The DFT computational models of (A) styrene, (B) nitrostyrene adsorption on the Au/TiO₂-EC catalyst, (C) enlarged image for clear observation of nitrostyrene adsorption on Au/TiO₂-EC catalyst.

Based on our computational models, it is quite different between styrene and nitrostyrene in terms of the adsorption positions. As for the styrene case, it appears that the styrene prefers to attach on the Au/TiO₂-EC through the carbon atoms of the C=C group (The most energetic favorable confirmation is shown in the Figure S11A). While for the nitrostyrene molecule, the adsorption occurs between the nitro group and the Au atoms close to the oxygen vacancy region (The most energetic favorable confirmation is shown in the Figures S11B and S11C). These results indicate that the nitrostyrene and nitrobenzene exhibit strong adsorption on the Au/TiO₂-EC *via* the nitro groups attaching on atoms close to the oxygen vacancy region. In contrast, this specific adsorption phenomenon is undetectable for -C=C groups adsorbed on the Au/TiO₂-EC, in good agreement with the results in IR spectra (Figures S8 and S9).

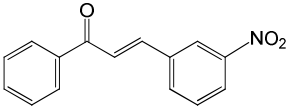
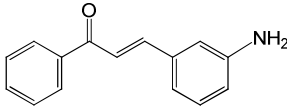
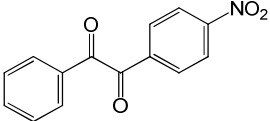
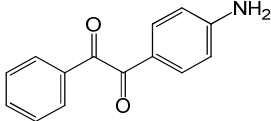
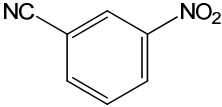
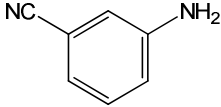
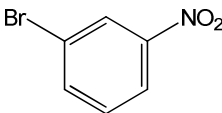
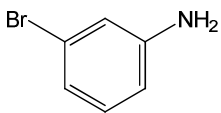
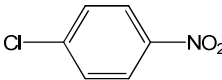
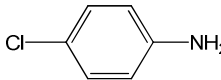
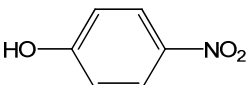
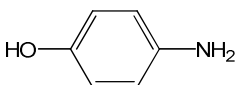


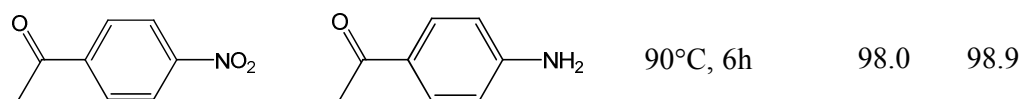
Scheme S1. Hydrogenation of nitroarenes to corresponding aniline products.



Scheme S2. Hydrogenation of 3-nitrostyrene to 3-aminostyrene in a 4.8-g scale system. Reaction conditions: 4.8 g of nitrobenzene, 30 bar of H₂, 0.9 g of Au/TiO₂-EC, 100 ml of toluene, 80 °C, and 6 h. The TOF was calculated over all the Au species in the reaction system in a reaction time of 20 min.

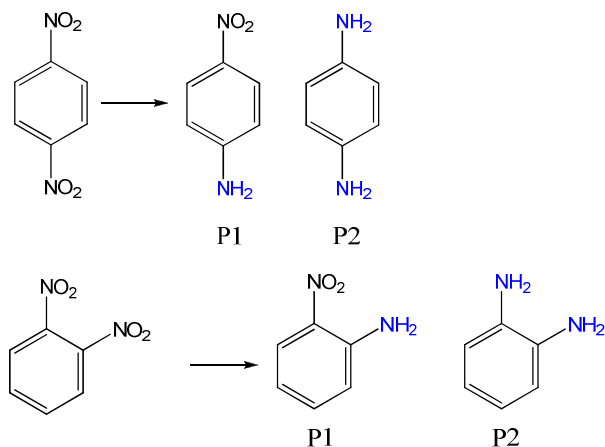
Table S1. Chemoselective hydrogenation of various substrates with H₂ over the Au/TiO₂-EC catalyst.^a

Reactant	Product	Conditions	Conv. (%)	Sel. (%)
		90°C, 4h	95.0	>99.5
		80°C, 4h	92.2	99.0
		100°C, 6.5h	95.0	97.9
		100°C, 6.5h	94.1	>99.0
		90°C, 4h	99.0	>99.5
		90°C, 4h	97.2	>99.5



^a Reaction conditions: 10 bar of H₂, 0.8 mmol of substrate, 40 mg of catalyst, and 3 ml of toluene.

Table S2. Catalytic data in the hydrogenation of dinitrobenzene over the Au/TiO₂-EC and Au/TiO₂-Con.^a



Entry	Substrate	Catalyst	Time (h)	Conv. (%)	Selectivity (%) ^b		
					P1	P2	P3
1	1,4-dinitrobenzene	Au/TiO ₂ -EC	4	84.2	65.0	24.1	<1.0
2		Au/TiO ₂ -EC	10	>99.0	14.5	85.5	-- ^c
3		Au/TiO ₂ -Con	4	41.7	96.9	3.0	<1.0
4		Au/TiO ₂ -Con	10	94.9	80.1	17.1	2.8
5	1,2-dinitrobenzene	Au/TiO ₂ -EC	4	97.5	69.9	29.8	<1.0
6		Au/TiO ₂ -EC	10	>99.0	25.7	73.6	<1.0
7		Au/TiO ₂ -Con	4	59.0	98.0	2.0	-- ^c
8		Au/TiO ₂ -Con	10	98.0	89.0	10.1	<1.0

^a Reaction conditions: 0.8 mmol of nitrobenzene, 40 mg of catalyst, 3 ml of toluene, 20 bar of H₂, 90 °C; ^b P1: mono-hydrogenation products; P2: bi-hydrogenation products; P3: nitrosonitrobenzene and some others; ^c Undetectable.

In the hydrogenation of 1,4-dinitrobenzene and 1,2-dinitrobenzene, Au/TiO₂-EC always gives higher conversion than Au/TiO₂-Con, in good agreement with those in the hydrogenation of other nitroarenes (Table 1 in the main-text). Notably, Au/TiO₂-EC and Au/TiO₂-Con both exhibit higher selectivities to mono-hydrogenation products (*o*- or *p*-nitroaniline) than bi-hydrogenation products (*o*- or *p*-phenylenediamine) in a short reaction time of 4 h (entries 1, 3, 5 and 7 in Table S2). When the reaction time was prolonged to 10 h, Au/TiO₂-EC gives major products of bi-hydrogenation products (entries 2 and 6 in Table S2) while the Au/TiO₂-Con still exhibit high selectivities to mono-hydrogenation products (entries 4 and 8 in Table S2). This phenomenon should be attributed to the strongly adsorption of nitro groups on Au/TiO₂-EC, which is favorable for the hydrogenation of nitro groups in di-nitro aromatic compounds.

References

1. Wang, L., Wang, H., Rice, A. E., Zhang, W., Li, X., Chen, M., Meng, X., Lewis, J. P., Xiao, F.-S. *J. Phys. Chem. Lett.* **2015**, 6, 2345-2349.
2. Fukui, K., Yonezawa, T., Shingu, H. *J. Chem. Phys.* **1952**, 20, 722-725.
3. Fukui, K., Yonezawa, T., Nagata, C., Shingu, H. *J. Chem. Phys.* **1954**, 22, 1433-1442.
4. Parr, R. G., Yang, W. T. *J. Am. Chem. Soc.* **1984**, 106, 4049-4050.
5. Yang, W. T., Parr, R. G. *Proc. Natl. Acad. Sci. U. S. A.* **1985**, 82, 6723-6726.
6. Yang, W. T., Parr, R. G., Pucci, R. *J. Chem. Phys.* **1984**, 81, 2862-2863.
7. Kohn, W., Becke, A. D., Parr, R. G. *J. Phys. Chem.* **1996**, 100, 12974-12980.
8. Lewis, J. P., Glaesemann, K. R., Voth, G. A., Fritsch, J., Demkov, A. A., Ortega, J., Sankey, O. F. *Phys. Rev. B.* **2001**, 64, 195103.
9. Shellman, S. D., Lewis, J. P., Glaesemann, K. R., Sikorski, K., Voth, G. A. *J. Comp. Phys.* **2003**, 188, 1-15.
10. Jelínek, P., Wang, H., Lewis, J. P., Sankey, O. F., Ortega, J. *Phys. Rev. B.* **2005**, 71, 235101.
11. Wang, H., Lewis, J. P. *J. Phys. Cond. Mat.* **2006**, 18, 421-434.
12. Wadati, H., Okazaki, K., Niimi, Y., Fujimori, A., Tabata, H., Pikus, J. Lewis, J. P. *Appl. Phys. Lett.* **2005**, 86, 023901.
13. Elliott, J., Starikov, E. B., Crawshaw, J., Claiden, P., Nilsson, L., Windle, A. *Modern methods for theoretical physical chemistry of biopolymers*. Elsevier, Amsterdam, **2006**, 407-428.
14. Wang, H., Stalnaker, J., Chevreau, H., Lewis, J. P. *Chem. Phys. Lett.* **2008**, 457, 26-30.